

## Supplementary Information (SI) for:

### Combined Charge Carrier and Photoelectrochemical Characterization of BiVO<sub>4</sub> Single Crystals: Intrinsic Behavior of a Complex Metal Oxide

Alexander J. E. Rettie,<sup>a</sup> Heung Chan Lee,<sup>b</sup> Luke G. Marshall,<sup>c</sup> Jung-Fu Lin,<sup>d</sup> Cigdem Capan,<sup>e</sup> Jeffrey Lindemuth,<sup>f</sup> John S. McCloy,<sup>g</sup> Jianshi Zhou,<sup>c</sup> Allen J. Bard<sup>b</sup> and C. Buddie Mullins<sup>a,b,c\*</sup>

<sup>a</sup> McKetta Department of Chemical Engineering, The University of Texas at Austin, TX 78712 (USA)

<sup>b</sup> Center for Electrochemistry, Department of Chemistry and Biochemistry, The University of Texas at Austin, TX 78712 (USA)

<sup>c</sup> Materials Science and Engineering Program, Texas Materials Institute, Department of Mechanical Engineering, The University of Texas at Austin, TX 78712 (USA)

<sup>d</sup> Department of Geological Sciences, The University of Texas at Austin, TX 78712 (USA)

<sup>e</sup> Department of Physics and Astronomy, Washington State University, Pullman, WA 99164 (USA)

<sup>f</sup> Lake Shore Cryotronics, Westerville, OH 43081 (USA)

<sup>g</sup> Energy and Environment Directorate, Pacific Northwest National Laboratory, Richland, WA 99354 (USA)

## Sample preparation

After growth, the crystal boules could be easily cleaved to reveal mirror-like (001) faces. These were cut with a diamond saw so that rectangular plate samples oriented with edges along the principal axes:  $a$ ,  $b$  or  $c$ , were obtained. As shown in the Laue XRD patterns in Figure 4, the  $a$  and  $b$  directions are highly symmetrical, which was expected as the BiVO<sub>4</sub> unit cell is a slightly distorted tetragonal structure (where  $a = b$ ). As the properties of interest were not expected to change significantly between  $a$  or  $b$ , it was not practical to differentiate between them and they were collectively termed  $ab$ .  $c$ -plates refer to samples where (001) is the main crystal face exposed (Figure S1) and the edges are along the  $a$  or  $b$  directions.  $ab$ -plates refer to samples where (100) or (010) is the main crystal face exposed (Figure S1) and one edge is along the  $c$  direction, while the other is along either  $a$  or  $b$ .

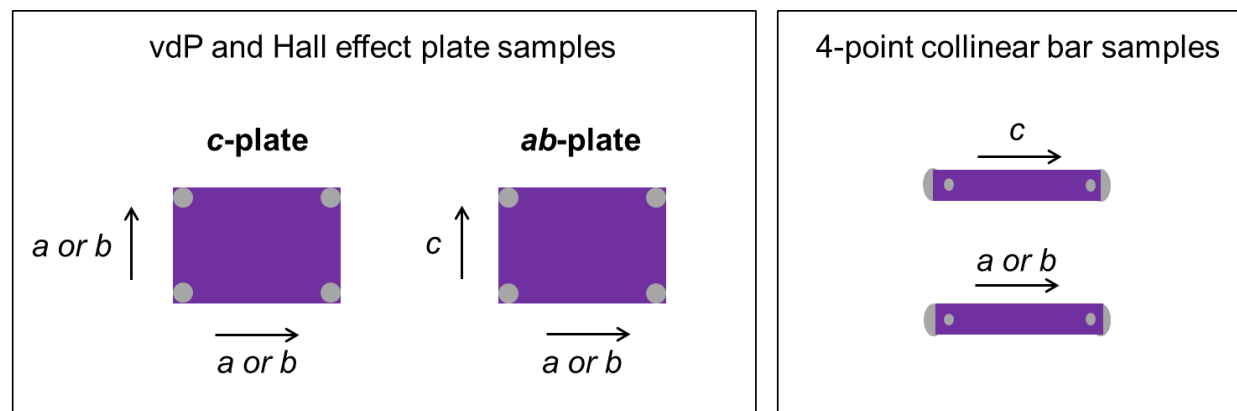


**Figure S1:** Diagram of various sample geometries. Arrows represent orientation relative to the principal crystallographic axes. Grey spots represent contact placement, which were connected to copper wire. The small inner contacts for the 4-point collinear samples were used for the voltage probes.

## Contact application

Small dots of liquid InGa eutectic (Sigma-Aldrich) were painted on the sample edges using a fine-tipped dental tool. Fine copper wires (California Fine Wire Company) were then stuck to the liquid dots and soldered to larger contact pads on a sample measurement board before Ag epoxy (Circuit Works) was applied over the wire and liquid InGa eutectic to hold it in place. Heat treatment in air at 150 °C for 15 mins was used to cure the Ag epoxy. Simply sticking the Cu wires to the liquid dots was observed to give Ohmic contacts with equivalent resistances but were not robust enough for repeated measurements or handling. For the Ag paste only contacts, the same procedure was employed only without painting on InGa eutectic. Indium metal pads were gently pressed into crystal surfaces that had been lightly roughened using sandpaper. All contact application was performed under an optical microscope with the sample held in place with double-sided tape (Scotch or Kapton). Figure S2 shows that the InGa eutectic contacts were the only ones that gave Ohmic behavior.

## Electrical measurements

For van der Pauw (vdP) resistivity experiments steady state 2- and 4-point voltage measurements were recorded at  $\pm 0.3$  and  $\pm 0.9$   $\mu\text{A}$  at all temperatures automatically using a custom graphical interface. These data were used to form  $i$ - $V$  curves (typical curve in Figure S3) at each temperature from which the resistance was obtained and used in the vdP formula.

In the AC field Hall measurements, a sinusoidal magnetic field with a frequency of 0.1 Hz was employed. The applied current is DC. Frequency dependent conductivity and Hall effect can be reasonably described using the Drude-Lorentz model. The time scale of this theory is determined by the mean free time between collisions. This time is so short (nano to picoseconds) compared to the AC field frequency that AC conductivity effects in the material can be ignored. The current was reversed to remove the inductive pickup signal from the Hall voltage.

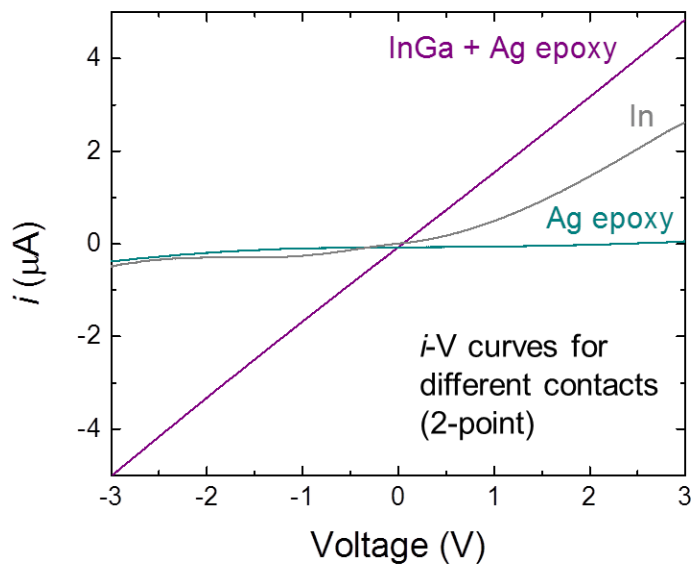


**Figure S2:** 2-point *i*-V curves at 300 K for various contacting methods employed. Only the InGa eutectic and Ag epoxy contact showed Ohmic behavior, while In metal pads showed diode behavior. Ag epoxy only was significantly more resistive and exhibited non-Ohmic behavior.

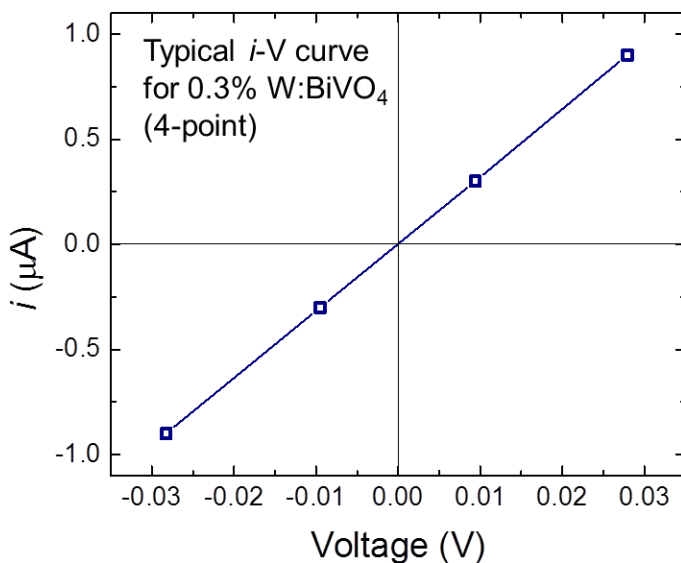


**Figure S3:** Typical 4-point *i*-V curve for resistance measurement at 300 K (in this case for a 0.3% W:BiVO<sub>4</sub> *c*-plate). Steady state voltages were measured at  $\pm 0.3$  and  $\pm 0.9$   $\mu$ A to generate the *i*-V curve (open symbols). The line is drawn between the points and is not fitted.

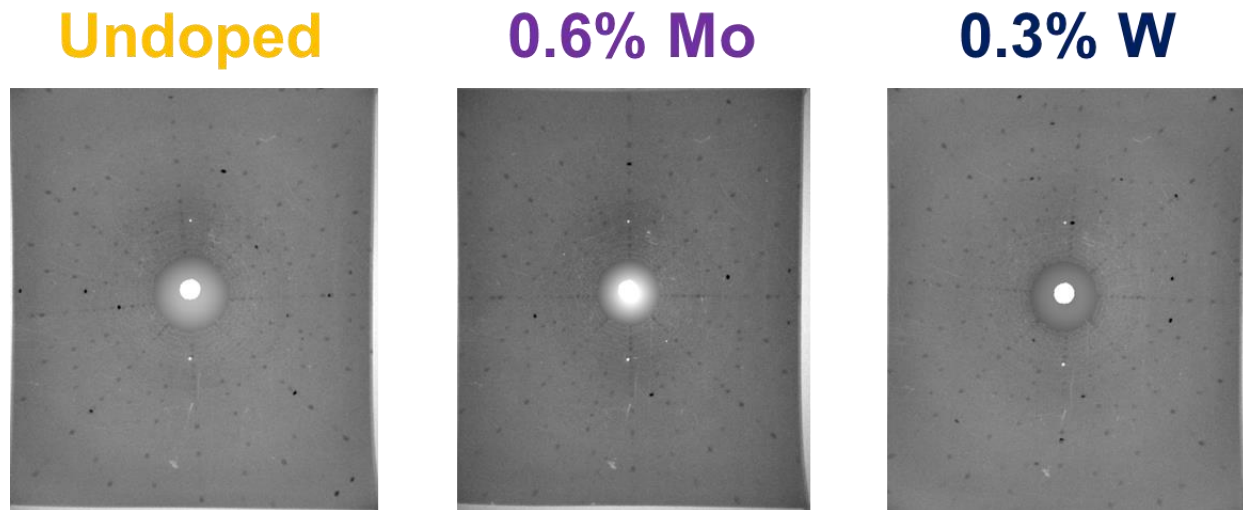


**Figure S4:** Typical Laue back-reflection patterns for an undoped and doped  $\text{BiVO}_4$  *c*-plate crystals (x-rays incident on the (001) face). To enhance the visibility of the Bragg peaks, the background pattern of the Laue image was fitted and stripped using a Mathematica image processing script.

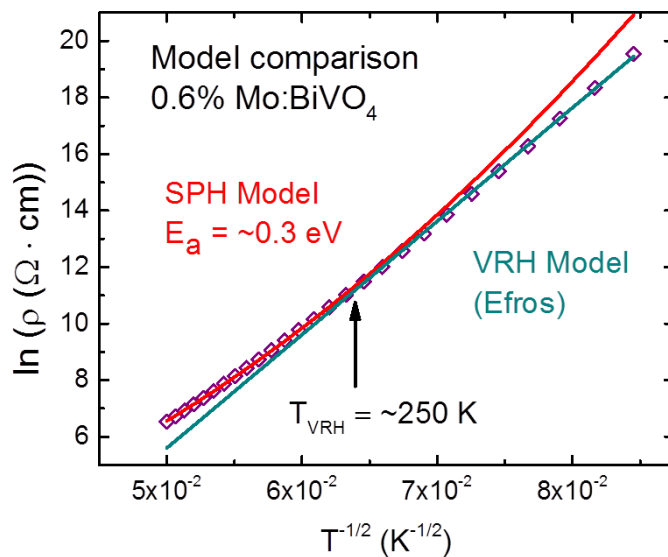


**Figure S5:** Fits of small polaron hopping (SPH) and variable range hopping (VRH) transport models to resistivity data. Arrow indicates transition to the VRH mechanism.

**Table S1:** Resistivity anisotropy of doped BiVO<sub>4</sub> *c*-plates (300 K) calculated using the Kazani *et al.*'s method [1]. vdP: van der Pauw.  $\rho_1$  and  $\rho_2$  refer to resistivities along different plate edges, cut along either *a* or *b*, which could not be differentiated between due to close structural symmetry.

Sample	Geometry	Technique	$\rho_1 / \rho_2$
0.3% W	<i>c</i> -plate	vdP	1.2
0.6% Mo	<i>c</i> -plate	vdP	1.3

### Calculation of resistivity anisotropy for 0.3% W:BiVO<sub>4</sub> bar samples

Resistivity was calculated using Equation S1,

$$\rho = \frac{Rl}{A} \quad (S1)$$

where,  $\rho$  is the resistivity,  $R$  is the resistance,  $l$  is the length between the voltage probes and  $A$  is the cross sectional area.

For the bars oriented in the *c* and *ab* directions, resistivities of  $2.53 \times 10^4$  and  $8.83 \times 10^3 \Omega \cdot \text{cm}$  respectively were obtained, resulting in an anisotropy ratio,  $\rho_c / \rho_{ab}$  of 2.9 at 300 K.

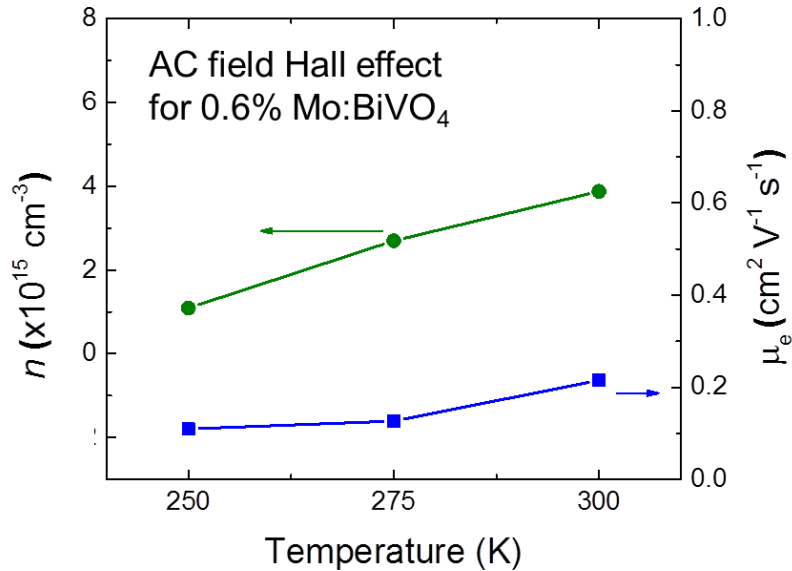


**Figure S6:** Carrier concentration ( $n$ ) and electron mobility ( $\mu_e$ ) AC field Hall effect as a function of temperature for a 0.6% W:BiVO<sub>4</sub> *c*-plate.

**Table S2:** vdP resistivity and AC field Hall effect data taken at 300 K. Two different 0.3% W samples were measured to check repeatability. \*this value was an average of 3 measurements (Table S3)

Sample	$\rho$ ( $\Omega$ -cm)	$n$ ( $\text{cm}^{-3}$ )	$\mu_e$ ( $\text{cm}^2 \text{V}^{-1} \text{s}^{-1}$ )
0.3% W (1)	$6.7 \times 10^3$	$4.7 \times 10^{15}$	0.20*
0.3% W (2)	$8.5 \times 10^3$	$4.9 \times 10^{15}$	0.15
0.6% Mo	$7.1 \times 10^3$	$4.8 \times 10^{15}$	0.18

**Table S3:** Repeated vdP resistivity and AC Hall effect measurements on 0.3% W:BiVO<sub>4</sub> c-plate sample 1 at 300 K.

Measurement	$\rho$ ( $\Omega$ -cm)	$n$ ( $\text{cm}^{-3}$ )	$\mu_e$ ( $\text{cm}^2 \text{V}^{-1} \text{s}^{-1}$ )
1	$6.6 \times 10^3$	$5.0 \times 10^{15}$	0.188
2	$6.7 \times 10^3$	$5.7 \times 10^{15}$	0.126
3	$6.7 \times 10^3$	$3.3 \times 10^{15}$	0.285
Average	$6.7 \times 10^3$	$4.7 \times 10^{15}$	0.200

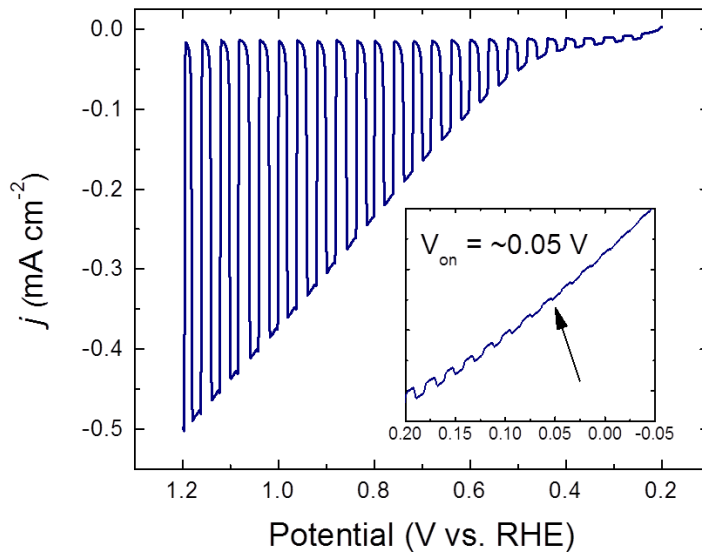


**Figure S7:** Linear sweep voltammogram under chopped illumination with a hole scavenger ( $\text{Na}_2\text{SO}_3$ ) using a W:BiVO<sub>4</sub> crystal with the (001) face exposed. The electrolyte solution was 0.1 M phosphate buffer with 0.1 M  $\text{Na}_2\text{SO}_4$  and 0.1 M  $\text{Na}_2\text{SO}_3$ . Inset shows on-set potential of  $\sim 0.05 \text{ V}$ .

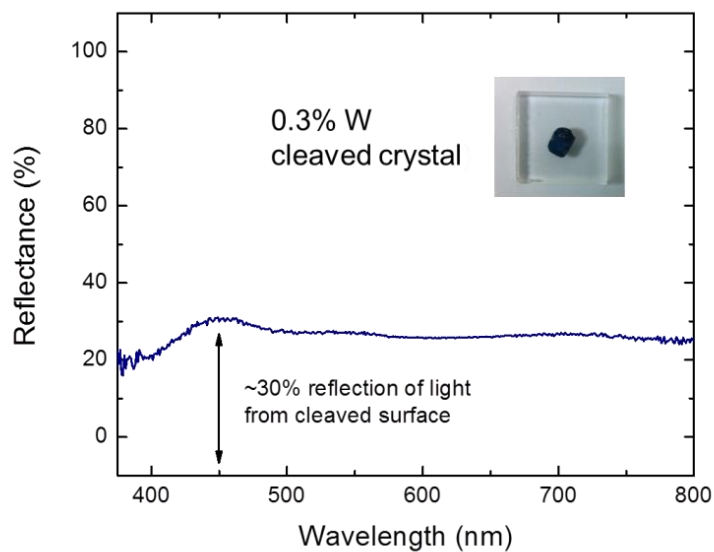


**Figure S8:** Diffuse reflectance spectra for a cleaved 0.3% W:BiVO<sub>4</sub> single crystal. Inset shows cleaved plate mounted on quartz.

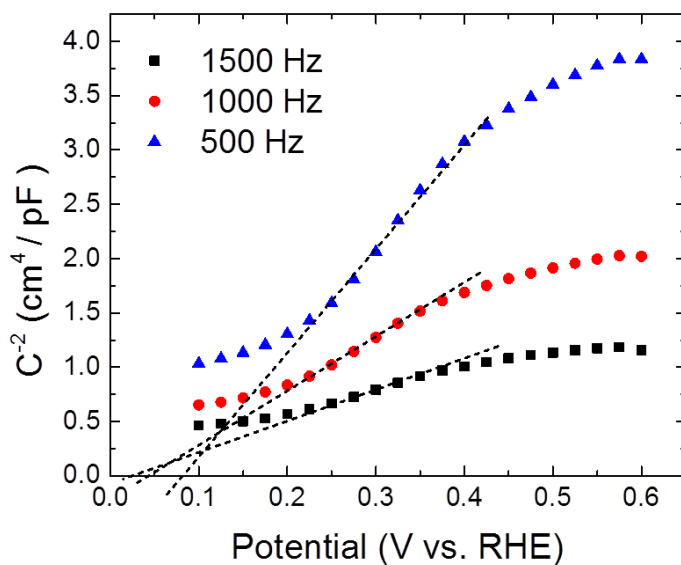


**Figure S9:** Mott-Schottky plots generated from capacitance-voltage data using a resistor and capacitor in series. The electrolyte solution was 0.1 M phosphate buffer with 0.1 M Na<sub>2</sub>SO<sub>4</sub> and the electrode was a W:BiVO<sub>4</sub> single crystal electrode.

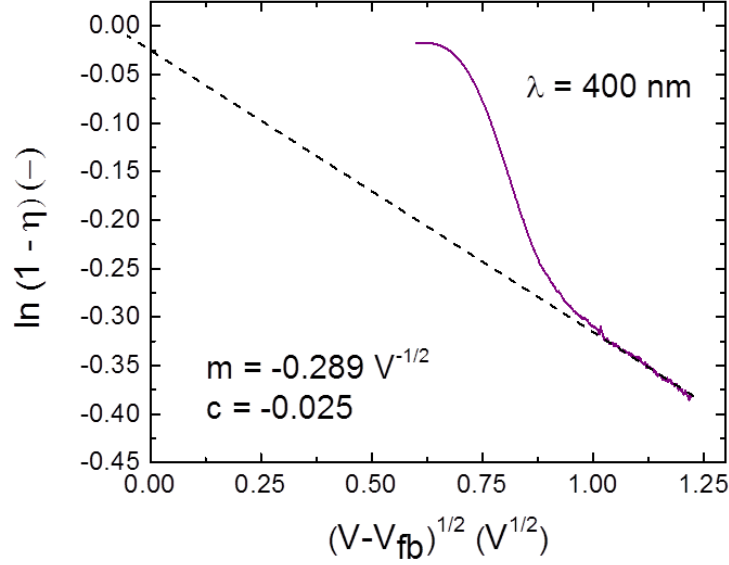


**Figure S10:** Determination of  $\alpha$  and  $L_p$  for a W:BiVO<sub>4</sub> single crystal electrode. The gradient ( $m$ ) and  $y$ -intercept ( $c$ ) of the linear region used in calculations are shown.  $\lambda = 400$  nm. The electrolyte solution was 0.1 M phosphate buffer with 0.1 M Na<sub>2</sub>SO<sub>4</sub> and 0.1 M Na<sub>2</sub>SO<sub>3</sub>.

### Calculation of hole diffusion length

LSVs using monochromated light were used to generate the plot in Figure S7. The electrolyte solution was 0.1 M phosphate buffer with 0.1 M Na<sub>2</sub>SO<sub>4</sub> and 0.1 M Na<sub>2</sub>SO<sub>3</sub>. The use of a hole scavenger is desired as we are interested in the electrical properties of the electrode bulk and want to minimize charge transfer limitations at the electrode surface. The surface of the crystals reflects ~20% of incident light at 400 nm (Figure S5) and this was accounted for in calculations of  $\eta$ . Optical losses through the glass cell window and aqueous electrolyte were not accounted for. Using the value of  $n$  at 300 K from AC field Hall effect measurements ( $n \sim 5 \times 10^{15} \text{ cm}^{-3}$ ),  $\alpha$  was determined as 2,620 cm<sup>-1</sup> using the gradient of the linear region and Equation 9 in the main text. The dielectric constant of undoped single crystals of BiVO<sub>4</sub> is 55 at 300 K [2] and was used in calculations.

**Table S4:** Comparison of metal oxide carrier mobility at 300K. Molecular beam epitaxy (MBE)

	Type	Growth method	Dopant	Orientation	$\mu$ (cm <sup>2</sup> V <sup>-1</sup> s <sup>-1</sup> )	Reference
TiO <sub>2</sub> (rutile)	Single crystal	Unclear	Reduction	c	1	3
TiO <sub>2</sub> (anatase)	Single crystal	Vapor transport	Reduction	c	10	4
$\alpha$ -Fe <sub>2</sub> O <sub>3</sub>	Epitaxial	MBE	Ti	$\perp$ c	0.1	5
$\gamma$ -WO <sub>3</sub>	Single crystal	Vapor transport	Reduction	Unclear	16	6
BiVO <sub>4</sub>	Single crystal	Floating zone	Mo, W	$\perp$ c	0.2	Our work

**Table S5:** Comparison of metal oxide hole diffusion lengths as determined by the Gärtner or equivalent model at 300 K.

	Type	Growth method	Dopant	Face exposed	$L_p$ (nm)	Reference
TiO <sub>2</sub> (rutile)	Single crystal	Unclear	Reduction	(001)	20	7
$\alpha$ -Fe <sub>2</sub> O <sub>3</sub>	Polycrystalline	Solid state reaction	Ti	-	2-4	8
$\gamma$ -WO <sub>3</sub>	Single crystal	Vapor transport	Reduction	Unclear	500	9
BiVO <sub>4</sub>	Single crystal	Floating zone	Mo, W	(001)	100	Our work

References in Tables S4 and S5: [3-9]

## References

1. Kazani, I., et al., *Van Der Pauw method for measuring resistivities of anisotropic layers printed on textile substrates*. Textile Research Journal, 2011. **81**(20): p. 2117-2124.
2. Akikatsu Sawada, T.F., *Electrical Properties of Ferroelastic Crystals with Scheelite Type Structure*. Toyota Kenkyu Hokoku, 1982(35): p. 6-11.
3. Cronemeyer, D.C., *Electrical and optical properties of rutile single crystals*. Physical Review, 1952. **87**(5): p. 876.
4. Forro, L., et al., *High mobility n-type charge carriers in large single crystals of anatase (TiO<sub>2</sub>)*. Journal of Applied Physics, 1994. **75**(1): p. 633-635.
5. Zhao, B., et al., *Electrical transport properties of Ti-doped Fe<sub>2</sub>O<sub>3</sub>(0001) epitaxial films*. Phys. Rev. B: Condens. Matter Mater. Phys., 2011. **84**: p. 245325/1-245325/9.
6. Berak, J.M. and M.J. Sienko, *Effect of oxygen-deficiency on electrical transport properties of tungsten trioxide crystals*. J. Solid State Chem., 1970. **2**: p. 109-33.
7. Finklea, H.O., *Semiconductor electrodes*. 1988: Elsevier Science Ltd.
8. Kennedy, J.H. and K.W. Frese, *Photooxidation of Water at  $\alpha$ -Fe<sub>2</sub>O<sub>3</sub> Electrodes*. Journal of the Electrochemical Society, 1978. **125**(5): p. 709-714.
9. Butler, M., *Photoelectrolysis and physical properties of the semiconducting electrode WO<sub>3</sub>*. Journal of Applied Physics, 1977. **48**: p. 1914.